Original Article

Effect of grain size on strength and strain rate sensitivity in the CrMnFeCoNi high-entropy alloy

Roberto B. Figueiredo [a],*, Witor Wolf [a], Terence G. Langdon [b]

[a] *Department of Metallurgical and Materials Engineering, Universidade Federal de Minas Gerais, Belo Horizonte, MG 31270-901, Brazil*
[b] *Materials Research Group, Department of Mechanical Engineering, University of Southampton, Southampton SO17 1BJ, UK*

ABSTRACT

It was shown recently that the grain size contribution to the flow stress and strain rate sensitivity of pure metals having different structures can be estimated by a model of deformation for grain boundary sliding. The present research extends this earlier study by estimating the grain size contribution to the flow stress in the CrMnCoFeNi high entropy alloy. This alloy has attracted significant attention in recent years due to its remarkable mechanical properties which include a higher strength compared to f.c.c. pure metals due to a significant contribution from solid solution strengthening. The present work demonstrates that the flow stress of the CrMnCoFeNi alloy can be readily estimated from the sum of the contributions from solid solution and grain size strengthening. There are some unique experimental trends observed in this alloy and these provide supporting evidence for the assumption that the grain size strengthening is thermally-activated. The flow stress, strain rate sensitivity, activation volume and activation energy are predicted for different grain sizes and testing conditions as a function of the fundamental properties of this alloy and the results show excellent agreement with the reported experimental data.

© 2022 The Author(s). Published by Elsevier B.V. This is an open access article under the CC BY-NC-ND license (http://creativecommons.org/licenses/by-nc-nd/4.0/).

1. Introduction

It was shown in a recent analysis [1] that an adjustment to the deformation mechanism of high temperature grain boundary sliding [2] permits a prediction of the deformation behavior of ultrafine-grained metals at low temperatures. Many of the deformation characteristics of these materials, including an absence of strain hardening, an increased strain rate sensitivity, the presence of grain boundary offsets and an increased vacancy concentration, are consistent with the basic assumptions of this deformation mechanism. Specifically, the model considers that extrinsic dislocations move along grain boundaries and activate dislocation slip in adjoining grains at places where there are stress concentrations such as triple junctions. These newly-activated dislocations then pile up at the opposite grain boundary and are removed by climb. Thus, the rate of deformation is controlled by the rate of grain boundary sliding and the rate of dislocation climb at the head of the pile up. It is well established that this mechanism predicts the deformation behavior of fine-

---

grained metals which display superplastic behavior at high temperatures. Furthermore, a recent comparison of experimental data also revealed excellent agreement for a number of different metals at low temperatures [1].

The fundamental deformation mechanism is based on the assumption that dislocations glide across the grains to the opposing grain boundaries. Thus, this condition is valid only in situations where there are no dislocation sub-structures within the grain interiors. In practice, this requirement is readily fulfilled for ultrafine and nanocrystalline materials since the grain sizes are then smaller than the stable sub-grain size and therefore dislocation cell formation is prevented. However, apart from ultrafine-grained metals, this condition is observed only in annealed coarse-grained metals where a dislocation substructure has not developed. In practice, therefore, this model can predict only the initial flow stress in regular coarse-grained annealed metals. Nevertheless, recent analyses [3,4] showed that this mechanism generally provides the best agreement with experimental data for the relationship between grain size and flow stress for a wide range of pure metals and grain sizes. The model also explains the trend of increasing strain rate sensitivity with decreasing grain size which is observed in most ultrafine-grained metals.

Despite the excellent agreement with experimental data for pure metals, the behavior of complex concentrated or high-entropy alloys (HEAs) has not been evaluated using this model. In addition, most of the mechanistic predictive theories published to date for face centered cubic (f.c.c.) HEAs are focused on solid solution effects and therefore they usually fail to include the grain size contribution in the models [5]. To overcome this deficiency, it is noted that the fundamental properties of a material which are used as the input parameters in the model, such as the shear modulus, the Burgers vector and the grain boundary diffusion coefficient, are expected to vary significantly among the different compositions of these multicomponent materials. Also, there are a very wide variety of compositions available and this introduces an added difficulty in attempting to compare experimental data from multiple sources.

Nevertheless, the CrMnFeCoNi alloy, known as the Cantor alloy [6] with the components listed in ascending order according to their atomic numbers, is the most studied of the f.c.c. HEA and it is an appropriate material for a detailed analysis. There are also reasonable sets of data available in the literature for this alloy including predictions of the shear modulus as a function of temperature [7] and the grain boundary diffusion parameters [8,9]. Accordingly, the present report concentrates exclusively on this alloy.

It is important to note also that the model for deformation by grain boundary sliding predicts only the effect of grain size on the deformation behavior of metals and the incorporation of a threshold stress is required to predict the behavior of metallic materials at low temperatures. This is of particular importance for multicomponent alloys since the solution strengthening plays a major role in determining the value of the flow stress. Models have been suggested for the prediction of the solid solution strengthening contribution as a function of the composition of these multicomponent alloys and they generally display good agreement with the experimental data [10–14].

The present analysis of the deformation behavior of the CrMnFeCoNi alloy incorporates the conventional model of grain boundary sliding and an empirical description of the solute strengthening effect. It is shown that this combination effectively predicts the flow stress and the strain rate sensitivity of this alloy for a broad range of grain sizes, testing temperatures and strain rates. It is shown also that some unique trends reported for this alloy, including a decrease in the strain rate sensitivity and the activation volume with decreasing grain size [15], differences in the evolution of the activation volume with temperature for samples with different grain sizes [16] and a pronounced increase in the activation energy for deformation with increasing temperature in a nanocrystalline alloy [17], are in direct agreement with the predictions of the proposed model.

2. Description of the model

The flow stress of single-phase metals depends on strengthening mechanisms which are affected by structural parameters such as the type and amount of solid solution alloying elements, the grain size and the dislocation density. The present analysis is focused on the initial flow stress of the CrMnFeCoNi HEA and it will not consider the effect of the dislocation density for hardening. Theories of the solution strengthening of f.c.c. complex concentrated alloys are now readily available [10–14]. A comparison with experimental data suggests that it is possible to estimate the stress contribution from the solid solution, σ_{ss}, at different temperatures and strain rates using the following relationship [18]:

$$\sigma_{ss} = \sigma_0 exp\left(-\frac{1}{0.51}\frac{RT}{\Delta E}ln\left(\frac{\dot{\varepsilon}_0}{\dot{\varepsilon}}\right)\right) \qquad (1)$$

where σ_0 is the stress contribution at a temperature of 0 K, R is the gas constant, T is the absolute temperature, ΔE is the activation energy barrier, $\dot{\varepsilon}_0$ is a reference strain rate (considered as 10^5 s^{-1} in the present analysis) and $\dot{\varepsilon}$ is the strain rate during deformation. The values of σ_0 and ΔE in a similar equation were determined recently for the CrMnFeCoNi HEA as ~254 MPa and ~109 kJ mol^{-1}, respectively [13]. However, an analysis of the experimental data suggests a larger value for the stress contribution at low temperatures. Therefore, the present analysis considered instead the parameters estimated directly from a best fit with the experimental data where these values are $\sigma_0 = 400$ MPa and $\Delta E = 110$ kJ mol^{-1}.

The effect of grain size on the flow stress, σ_{gs}, may be estimated from the relationship [1]:

$$\sigma_{gs} = \sqrt{\frac{3GkT}{2db^2}ln\left(\frac{\dot{\varepsilon}d^3}{10\delta D_{gb}}+1\right)} \qquad (2)$$

where G is the shear modulus, k is Boltzmann's constant, d is the spatial grain size, b is the Burgers vector given by $b = 0.254$ nm [10], δ is the grain boundary width and D_{gb} is the coefficient for grain boundary diffusion. The grain boundary width is usually taken as $\delta = 2 \times b$ and this agrees with the value of $\delta \approx 0.5$ nm reported in the literature [8,9]. The shear

modulus of the CrMnFeCoNi alloy was evaluated over a range of temperatures and this gave the following relationship [7]:

$$G = 85 - \frac{16}{(e^{448/T} - 1)} \tag{3}$$

where T is the temperature in degrees K and the value of G is in GPa.

The coefficient for grain boundary diffusion is given by the following eq. (4):

$$\delta D_{gb} = \delta D_0 exp\left(\frac{-Q_{gb}}{RT}\right) \tag{4}$$

where the values for the various constants were estimated for the different elements in the CoCrFeMnNi alloy [8,9] and these values are given in Table 1. In practice, the grain boundary diffusion coefficient is similar for all elements at high temperatures but a lower value is observed for the diffusion of Ni at low temperatures. Nevertheless, the differences in the grain boundary diffusion coefficients for the different elements have no significant effect on the predictions from eq. (2). However, slightly better agreement with the experimental data was observed when using the values of diffusion for Ni and therefore these values were considered in the present analysis.

Thus, the flow stress, σ, of the CrMnFeCoNi HEA is estimated using the following eq. (5) which is obtained from the sum of the solid solution strengthening given by eq. (1) and the grain size strengthening given by eq. (2):

$$\sigma = \sigma_0 exp\left(-\frac{1}{0.51}\frac{RT}{\Delta E}ln\left(\frac{\dot{\varepsilon}_0}{\dot{\varepsilon}}\right)\right) + \sqrt{\frac{3GkT}{2db^2}ln\left(\frac{\dot{\varepsilon}d^3}{10\delta D_{gb}} + 1\right)} \tag{5}$$

3. Validation of the model

Experimental data from the literature [13,16,17,19−34] were used to validate the model and these data are summarized in Table 2 where it is evident that results were collected for a wide range of grain sizes, strain rates and temperatures. The present model considers the spatial grain size but the majority of these data evaluate the grain size using 2D-sections so that there will be some level of inaccuracy for this parameter. Thus, the values reported for the grain sizes were considered in the present analysis except for those reports defining clearly the use of the mean linear intercept length and for these reports the spatial grain size was estimated by multiplying the linear length by a factor of 1.74 [35]. These values are marked with an asterisk (*) in Table 2.

Table 1 − Grain boundary diffusion parameters for the different elements in the CrMnFeCoNi alloy.

	δD_0 (10^{-12} m^3/s)	Q_{gb} (kJ/mol)	Reference
Co	1.66	181.5	[7]
Cr	1.43	180.6	[7]
Fe	1.40	182.2	[7]
Mn	13	192.1	[7]
Ni	142	221	[8]

Table 2 − Summary of the experimental data used in the present analysis: asterisks in the grain size column denote the conversion from mean linear intercept to the spatial grain size.

d (µm)	T (K)	$\dot{\varepsilon}$ (s^{-1})	Reference
7.7*−270*	77−1073	10^{-3}	[18]
60.9*	77−1273	$10^{-3}/10^{-1}$	[32]
6	77/293	10^{-3}	[26]
0.05/10	293	10^{-3}	[20]
1	873−1073	$10^{-3}−10^{-1}$	[21]
1.4	1023	$10^{-4}−10^{-1}$	[22]
0.88*−155*	293	10^{-3}	[25]
131	77/293	10^{-3}	[33]
0.05	293−673	5×10^{-2}	[15]
0.036	298−573	2.5×10^{-2}	[16]
17	77−423	10^{-3}	[12]
0.06	293	10^{-2}	[24]
0.05	293	10^{-4}	[23]
0.5	77/293	10^{-3}	[27]
9.1	293	$3 \times 10^{-4}−2.8 \times 10^3$	[28]
23.9	293	$2 \times 10^{-4}−9.7 \times 10^2$	[29]
6.8* ~ 52.2*	293	10^{-3}	[30]
0.52/11	77−573	10^{-3}	[31]
1.1* ~ 183*	77−873	10^{-3}	[19]

Fig. 1 shows the predicted flow stress at a strain rate of 10^{-3} s^{-1} for the three different testing temperatures of 77, 293 and 1073 K plotted as a function of the grain size where the experimental data are taken from the literature for similar testing conditions [13,19−22,24−33]. It is readily apparent that there is an excellent agreement between the predictions from the model and the experimental data and this includes both the larger contributions of the solid solution and grain size strengthening mechanisms at lower testing temperatures and the occurrence of grain refinement softening at the highest temperature.

Fig. 2 shows the predicted flow stress as a function of strain rate for samples tested with different grain sizes at three different temperatures. The predictions are again compared with experimental data [23,29,30] and there is a good agreement for both the values of the flow stress and the slopes of the curves. From these plots, the slopes of the curves provide the values of the strain rate sensitivity, $m = \partial ln\sigma/\partial ln\dot{\varepsilon}$. Thus, the model predicts, in agreement with the experiments, a small strain rate sensitivity at room temperature and a larger value of m for fine-grained material tested at a high temperature. Careful inspection of the predictions of the model suggests a very small increase in the strain rate sensitivity with increasing grain size when testing at room temperature and this agrees with the experimental data as discussed in Section 4.1. The high strain rate sensitivity predicted for the high temperature testing of the fine-grained CrMnFeCoNi HEA is consistent with reports of superplastic elongations under these conditions [22,23].

The predicted evolution of the flow stress as a function of the testing temperature is depicted in Fig. 3 for three different grain sizes together with experimental data from the literature [16,19]. Different trends are revealed as the nano-crystalline material with d = 0.05 µm displays a lower dependence on temperature at low temperatures (T < 700 K)
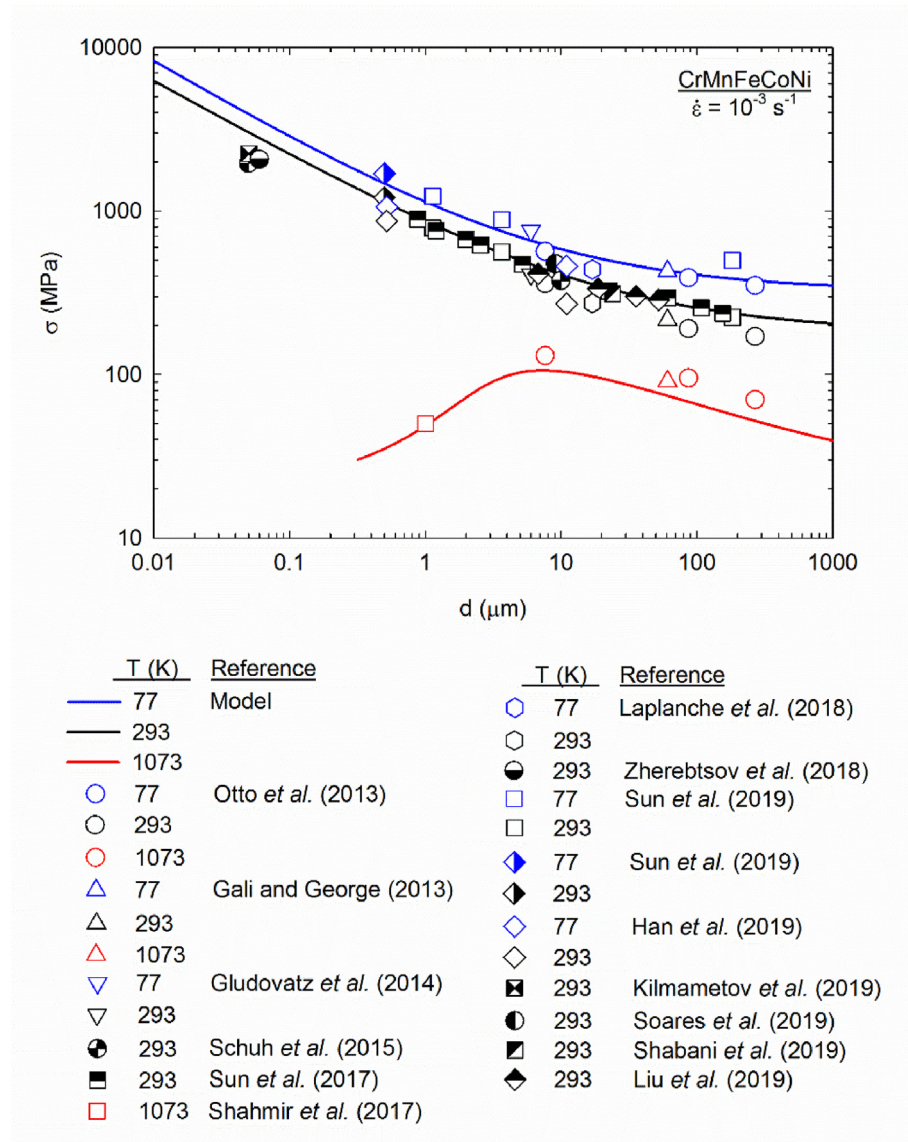
Fig. 1 − Predicted flow stress plotted as a function of grain size for three different temperatures: experimental data are shown for comparison [12,18−21,23−32].

and a pronounced drop in stress at intermediate temperatures (T > 700 K). The coarse-grained material with $d = 270$ μm displays a larger dependence of flow stress on temperature at low temperatures and the slope decreases at high temperatures. The fine-grained sample with $d = 7.6$ μm displays an intermediate behavior. All of the experimental data are consistent with the predictions from the model.

Fig. 4 shows the flow stress predicted by the model compared with results reported from experiments conducted with samples having different grain sizes tested at different temperatures and strain rates [13,16,17,19−34]. Two conclusions became apparent during the analysis of the data.

First, the levels of the flow stress observed in nanocrystalline CrMnFeCoNi alloys processed by HPT [16,17,21,24,25] are consistently slightly lower than predicted by the model and they do not follow the exact trend of grain refinement hardening observed in coarse-grained samples at room

temperature. This difference is probably associated with the experimental determinations of grain size using 2D-images from transmission electron microscopy (TEM) where the spatial grain size may be underestimated. Thus, the variation of flow stress with grain size in the nanocrystalline range is steeper than in the coarse-grained range.

Second, the levels of flow stress reported for the CrMnFeCoNi alloy tested at moderate temperatures in the range of 473−873 K tend to be larger than the values predicted by the model and this trend is more pronounced in the fine-grained samples. It is important to note that the formation of different phases was reported in this alloy in this temperate range and this is associated with a significant increase in strength [21]. However, such structural changes are not predicted by the model which considers only solid solution strengthening and grain size strengthening in a single-phase alloy. Despite these minor inconsistencies, there is generally
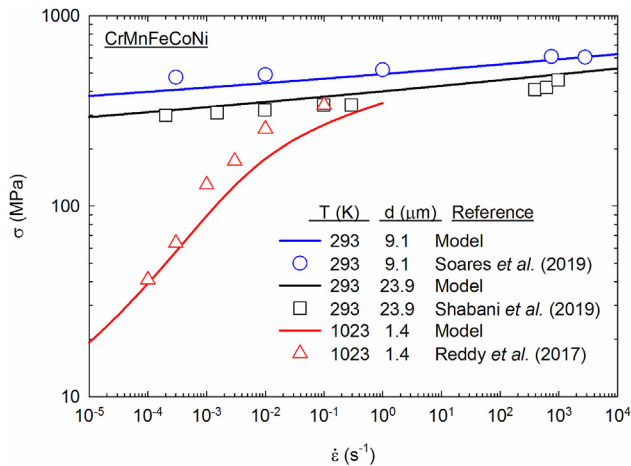
Fig. 2 – Predicted flow stress plotted as a function of the strain rate for three different grain sizes and temperatures: experimental data are also shown [22,28,29].

very good agreement between the model and experimental data as documented in Fig. 4.

4. Analysis of the deformation behavior of the CrMnFeCoNi alloy

4.1. Strain rate sensitivity

An intriguing aspect of the deformation behavior of the CrMnFeCoNi alloy is the increase in the strain rate sensitivity with increasing grain size for tests conducted at room temperature [15]. This trend is the opposite of that observed in conventional f.c.c. metals [36]. It has been shown that the pronounced increase in the strain rate sensitivity of many

f.c.c. metals in the ultrafine and nanocrystalline grain size ranges is readily explained by the mechanism of grain boundary sliding [1,3] and the analysis in the preceding section suggests that a similar explanation is appropriate also for the CrMnFeCoNi alloy. However, the present analysis demonstrates that the solid solution strengthening mechanism also plays an important role in the deformation behavior of this alloy. Therefore, it follows that the inverse relationship between the strain rate sensitivity and grain size may be a direct consequence of the enhanced contribution of solid solution strengthening in CrMnFeCoNi alloys at the coarser grain sizes compared to other f.c.c. metals. This possibility is now examined.

The present analysis is based on a combination of grain size strengthening and solid solution strengthening and both of these mechanisms are thermally-activated and dependent on the strain rate. In fine-grained pure f.c.c. metals tested at room temperature, the strain rate sensitivity is basically controlled by the grain boundary sliding mechanism given by eq. (2) which is then responsible for the grain size strengthening. This mechanism predicts an increase in the strain rate sensitivity with decreasing grain size whereas the solid solution strengthening is given by eq. (1) and is independent of the grain size. The strain rate sensitivity predicted by solid solution strengthening is larger than the value predicted by grain size strengthening for the CrMnFeCoNi alloy at low temperatures. For example, the strain rate sensitivity predicted by the solid solution strengthening mechanism is approximately 0.04 at room temperature. The strain rate sensitivity predicted by the grain size strengthening mechanism increases with decreasing grain size but is limited to values lower than ~0.01 at this temperature. Thus, coarse-grained alloys display a large strain rate sensitivity due to the large contribution of solid solution strengthening to the total strength. However, the ratio of the contribution from this mechanism decreases with decreasing grain size due to
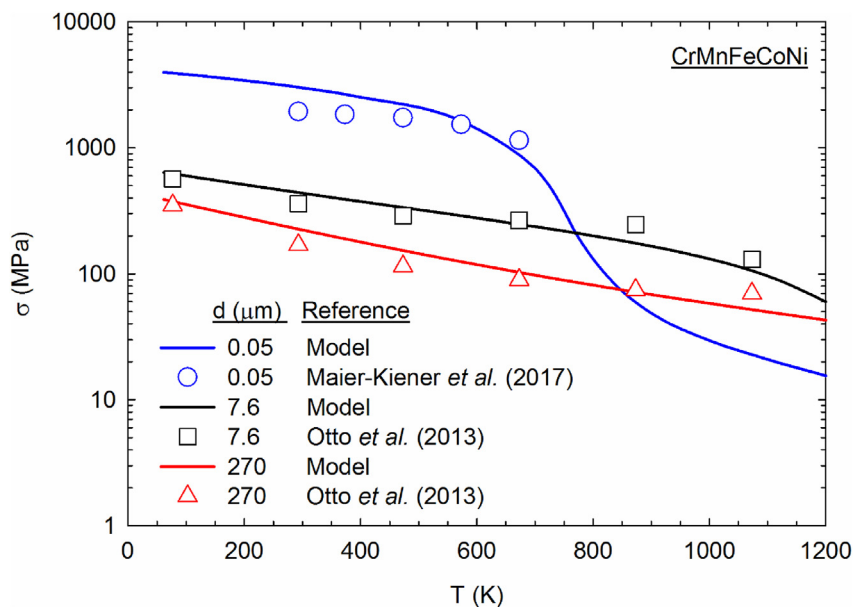

Fig. 3 – Predicted flow stress plotted as a function of the testing temperature for three different grain sizes: experimental data are also shown [15,18].
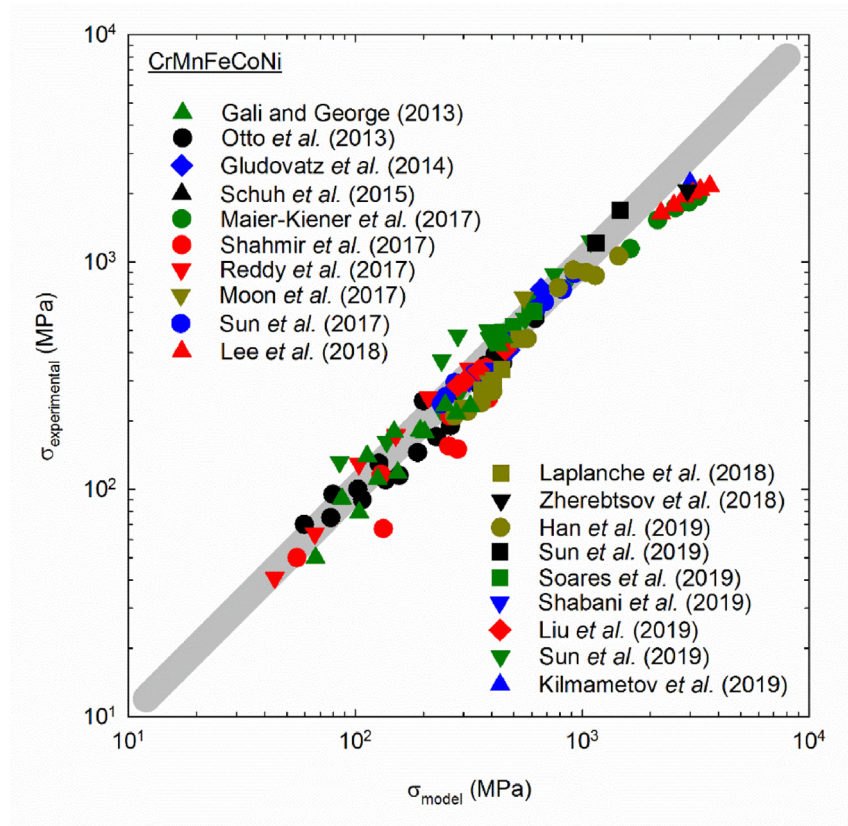
Fig. 4 − **Flow stress predicted by the model compared with the flow stresses reported from numerous experiments [12,15,16,18−33].**

the increased contribution of grain size strengthening and therefore the contribution of solid solution strengthening to the strain rate sensitivity also decreases. This is illustrated in Fig. 5 which shows the strain rate sensitivity predicted by the present model, for room temperature deformation at a strain rate of 10^{-3} s^{-1} plotted as a function of the grain size. Thus, values of $m \approx 0.01$ are predicted for ultrafine and nanocrystalline materials but this value increases to m > 0.02 for
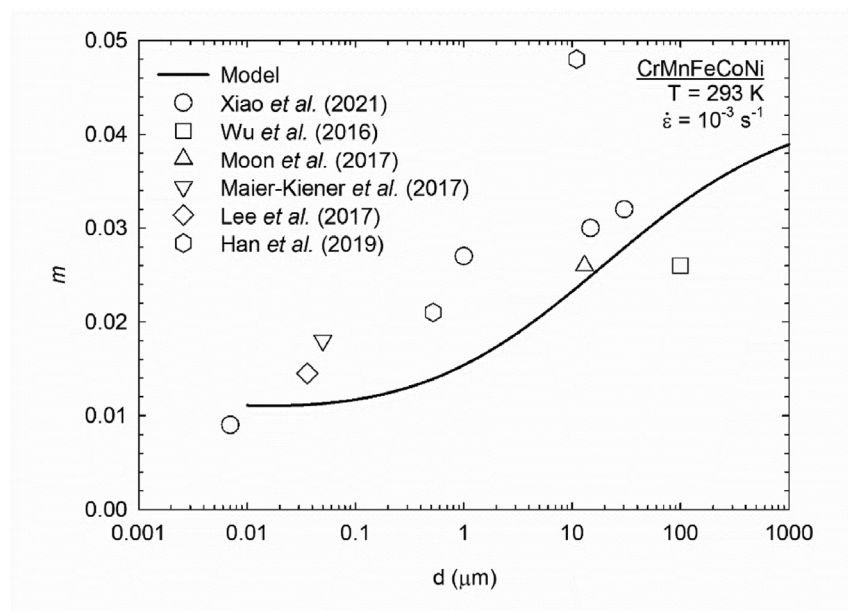

Fig. 5 − **The strain rate sensitivity predicted for deformation at room temperature plotted as a function of the grain size: experimental data are also shown [14−16,31,33,36].**
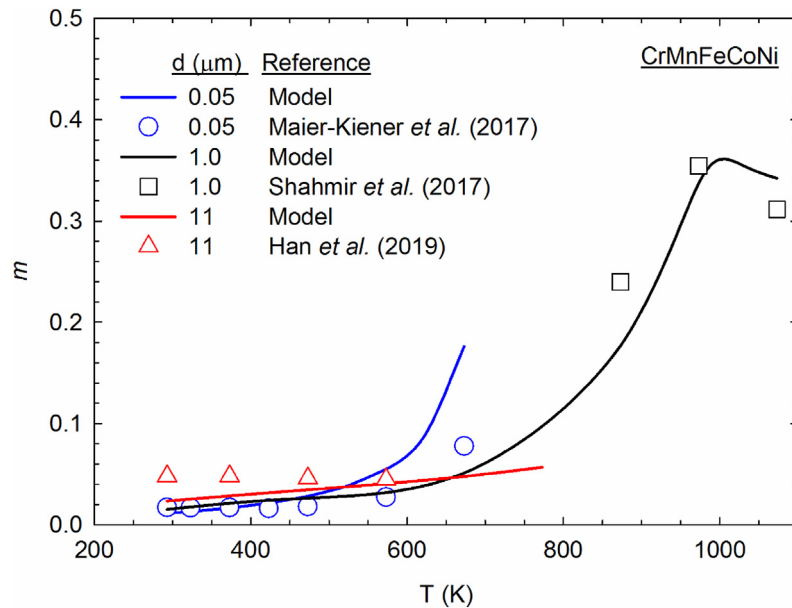
Fig. 6 – The strain rate sensitivity predicted for three different grain sizes plotted as a function of temperature: experimental data are also shown [15,21,31].

grain sizes larger than ~1 μm. The values of the strain rate sensitivity determined experimentally [15−17,32,34,37] are also plotted in Fig. 5 and generally they show reasonable agreement with the predictions of the model.

With increasing temperature the strain rate sensitivity predicted by the grain boundary sliding mechanism increases significantly for small grain sizes. Ultimately, a value of $m \approx 0.5$ is expected for this mechanism at high temperatures and low strain rates in fine-grained materials and this is associated with the occurrence of conventional superplasticity [38]. Therefore, the strain rate sensitivity of fine grained CrMnFeCoNi alloys will be larger than the values reported for their coarse-grained counterparts at high temperatures. This is depicted in Fig. 6 which shows the strain rate sensitivity predicted by the model for the three different grain sizes of nanocrystalline ($d = 0.05$ μm), fine ($d = 1$ μm) and relatively coarser ($d = 11$ μm) grain sizes plotted as a function of the temperature for a strain rate of 10^{-3} s^{-1}. Thus, the values predicted for the finer grain sizes are smaller at low temperatures but they become significantly larger at higher temperatures. Experimental data are also shown in Fig. 6 [16,22,32] and these experimental points confirm the overall predictions. Thus, an increase in the strain rate sensitivity up to close to $m \approx 0.10$ was reported in a nanocrystalline material tested up to 673 K [16] and this value is larger than the values reported for the coarser-grained alloy.

It is important to note also that the significant contribution of solid solution strengthening in the CrMnFeCoNi alloy appears to compromise the maximum strain rate sensitivity that may be achieved in this material at high temperatures. While strain rate sensitivities in the range of ~0.4−0.5 are usually observed at high temperatures in fine-grained superplastic metals, the maximum values predicted by the present model are usually limited to $m < 0.4$. This is depicted in Fig. 6 where the prediction of m for a sample with a grain

size of 1 μm is a maximum of $m \approx 0.35$ at T ≈ 1000 K. Nevertheless, it should be noted that this value of m is fully consistent with experimental results for a fine-grained CrMnFeCoNi alloy where there was superplastic flow and a measured relatively low strain rate sensitivity of $m \approx 0.30$ for tests conducted over strain rates of $10^{-3}-10^{-1}$ s^{-1} at temperatures in the range of 873−1073 K [22]. In the earlier experiments the low strain rate sensitivity recorded in an alloy exhibiting superplastic elongations of >600% was tentatively attributed to the occurrence of significant grain growth during the tensile testing [22] but the present analysis suggests an alternative explanation.

4.2. Activation volume and the activation energy

In order to gain a better understanding of the deformation mechanisms, the activation volumes and activation energies are usually determined in appropriate experiments. The activation volume, V, may be estimated by testing at different strain rates and using the following eq. (6):

$$V = \sqrt{3}kT\frac{\partial ln\dot{\epsilon}}{\partial \sigma} = \frac{\sqrt{3}kT}{m\sigma} \qquad (6)$$

It can also be estimated for the model by comparing the predictions for different testing strain rates.

The present model essentially comprises a combination of two thermally-activated deformation mechanisms. Although grain size strengthening is usually considered athermal, some earlier reports considered this mechanism as thermally-activated [1,3] and this approach demonstrated an excellent agreement between the model and experimental data for different metals at different temperatures and strain rates. Also, the following analysis provides additional supporting evidence that the grain size strengthening mechanism is thermally-activated.
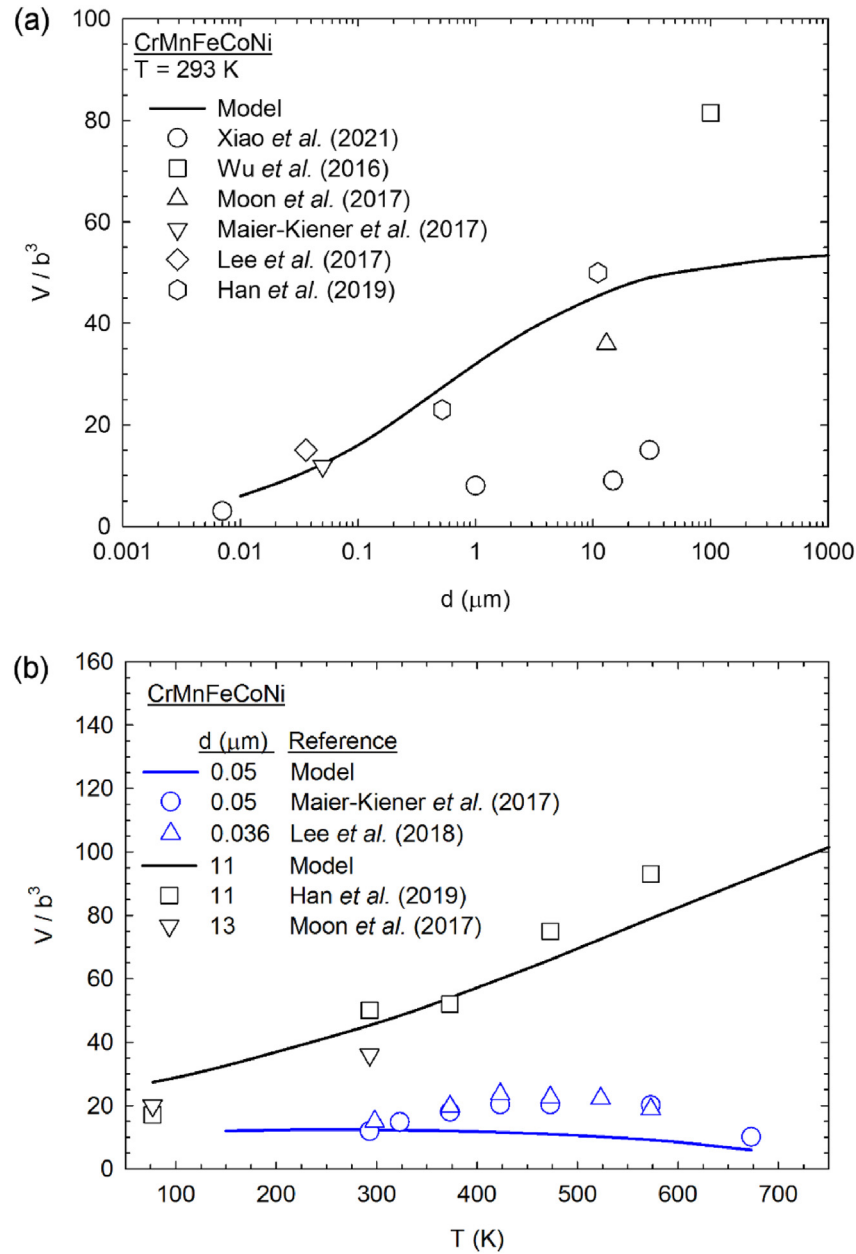
Fig. 7 − Prediction of the activation volume as a function of (a) the grain size and (b) the temperature; experimental data are also shown [14−16,31,33,36].

The activation volume associated with the solid solution strengthening mechanism is expected to be independent of the grain size. Thus, considering an athermal grain size strengthening contribution of the type $\sigma = k'd^{-1/2}$ where k' is a constant, the activation volume predicted by the model is independent of the grain size. For example, a value of $V \approx 55\ b^3$ is predicted for deformation at room temperature at a strain rate of $10^{-3}\ s^{-1}$ for all grain sizes. However, when two thermally-activated mechanisms are summed, the predicted activation volume becomes $1/V = 1/V_1 + 1/V_2$ where V_1 and V_2 are the activation volumes for each separate mechanism. Consequently, the predicted activation volume will always be slightly smaller than the smallest value for the different mechanisms.

The activation volume predicted by the grain size strengthening mechanism modeled by eq. (2) decreases with decreasing grain size. As a consequence, the activation volume predicted for the present model by eq. (5) decreases at small grain sizes but saturates at ~55 b^3 at large grain sizes for deformation at room temperature as depicted in Fig. 7a. This trend of decreasing activation volume with decreasing grain size was observed experimentally in the reported data [15−17,32,34,37] as also included by the points in Fig. 7a that show a generally good agreement with the prediction.

The activation volumes predicted by the present model also display different evolutions with temperature depending upon the grain size. Although the solid solution strengthening mechanism predicts an increase in activation volume with
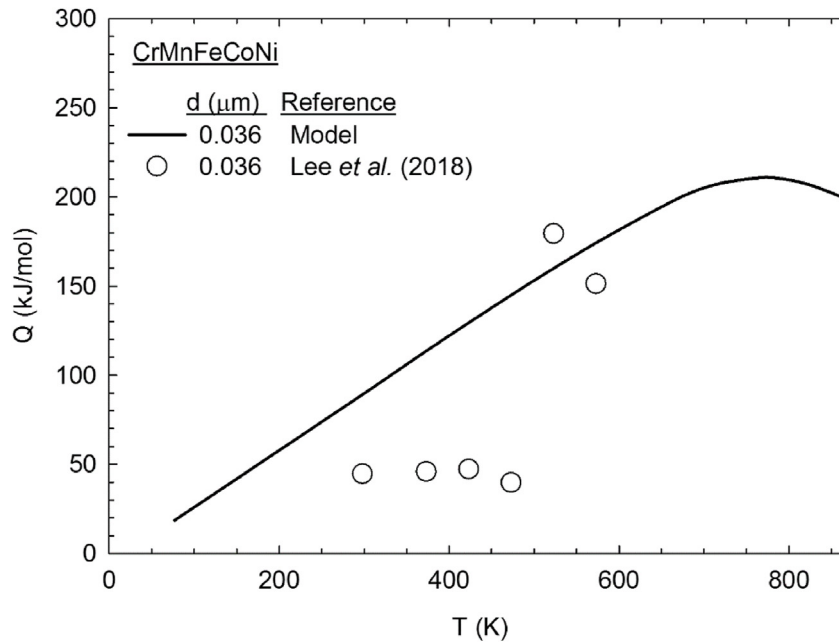
Fig. 8 − **The predicted activation energy plotted as a function of the testing temperature: experimental data ae also included [16].**

increasing temperature [13], the grain size strengthening mechanism predicts different trends depending on the grain size. Therefore, the latter mechanism plays a key role in governing the evolution of this parameter for fine-grained materials. Fig. 7b shows the predicted V as a function of temperature considering samples with different grain sizes that may be categorized as either nanocrystalline material with grain sizes close to ~0.05 μm or relatively coarser-grained material with grain sizes of the order of ~11 μm. There is a clear increase in the predicted values of the activation volumes with increasing temperature for the coarser-grained material and this is in excellent agreement with the experimental data. Conversely, a smaller and near constant value of V is predicted for the nanocrystalline material and again this trend agrees with the experimental data.

The activation energies for deformation, Q, are also determined in experiments and the following eqs. (7) and (8) are usually used for this determination by conducting tests at different temperatures. Specifically, the relationship in eq. (7) relates to testing at constant stress and the relationship in eq. (8) relates to testing at a constant strain rate:

$$Q = RT^2 \frac{\partial \dot{\varepsilon}}{\partial T} \tag{7}$$

and

$$Q = nR \frac{\partial \ln \sigma}{\partial (1/T)} \tag{8}$$

where n is the stress exponent defined as $1/m$.

Both eqs. (7) and (8) can be used to estimate the activation energy predicted by the model and thereby they permit a direct comparison of predictions at different temperatures for a constant grain size. In practice, the model predicts an increase in the activation energy at low temperatures but

the slope varies for different grain sizes such that higher slopes are predicted for smaller grain sizes. The model also predicts a maximum value for the activation energy of ~220 kJ mol^{-1} at high temperatures and this is the value considered in the present model for the activation energy for grain boundary diffusion.

Fig. 8 shows the predicted activation energy for a nanocrystalline material having a grain size of $d = 0.036$ nm plotted as a function of temperature and including experimental data [17]. Thus, the prediction agrees with the experimental data for the tests conducted at temperatures of 523−573 K but at lower temperatures the prediction overestimates the values of Q. It is important to note that mechanical testing of the CrMnFeCoNi HEA at moderate temperatures may be affected by the precipitation of different phases that will increase the strength of the material and this effect will be observed primarily in materials having finer grain sizes. This is supported by the increase in hardness reported in nanocrystalline samples of this alloy after heating at moderate temperatures [16,21]. Also, an increase in yield stress with increasing testing temperature was reported in an ultrafine-grained sample of the alloy in the temperature range of 300−473 K [32]. This shows that the experimental activation energies determined by mechanical testing at moderate temperatures may underestimate the true values due to these microstructural changes and this will directly explain the apparent low values of the activation energies recorded experimentally in Fig. 8 at the lower testing temperatures.

5.   Summary and conclusions

1. The flow stress, strain rate sensitivity, activation volume and activation energy of the CrMnFeCoNi high-entropy

alloy were modeled by considering the contribution of two thermally-activated strengthening mechanisms which predict the separate contributions of solid solution strengthening and grain size strengthening. A generally excellent agreement is observed between the model and experimental data for different testing conditions including a wide range of grain sizes, strain rates and testing temperatures. This agreement is achieved without the use of any adjustable parameters.

2. The analysis demonstrates that the mechanism of grain boundary sliding, which was shown earlier to give excellent agreement with data for conventional single phase metals, agrees also with the experimental observations in this multicomponent alloy.

3. The trend in this alloy for decreasing strain rate sensitivity with decreasing grain size, which is the opposite to conventional f.c.c. metals, is readily explained by the enhanced contributions from solid solution strengthening for the coarser-grained materials and grain size strengthening for the fine-grained materials.

4. The trend observed experimentally of decreasing activation volume with decreasing grain size is in agreement with the present model and provides supporting evidence that the grain size strengthening is thermally-activated.

5. The model predicts an increase in the activation energy with increasing testing temperature so that large values are predicted at moderate temperatures and this agrees with values determined experimentally.

Data availability

The raw/processed data required to reproduce these findings cannot be shared at this time due to technical or time limitations.

Declaration of Competing Interest

The authors declare that they have no known competing financial interests or personal relationships that could have appeared to influence the work reported in this paper.

Acknowledgements

REFERENCES

[1] Figueiredo RB, Langdon TG. Deformation mechanisms in ultrafine-grained metals with an emphasis on the Hall-Petch relationship and strain rate sensitivity. J Mater Res Technol 2021;14:137–59.

[2] Langdon TG. A unified approach to grain boundary sliding in creep and superplasticity. Acta Metall Mater 1994;42(7):2437–43.

[3] Figueiredo RB, Langdon TG. Effect of grain size on strength and strain rate sensitivity in metals. J Mater Sci 2022;57:5210–29.

[4] Figueiredo RB, Edalati K, Langdon TG. Effect of creep parameters on the steady-state flow stress of pure metals processed by high-pressure torsion. Mater Sci Eng, A 2022;835:142666.

[5] George EP, Curtin WA, Tasan CC. High entropy alloys: a focused review of mechanical properties and deformation mechanisms. Acta Mater 2020;188:435–74.

[6] Cantor B. Multicomponent high-entropy Cantor alloys. Prog Mater Sci 2021;120:100754.

[7] Laplanche G, Gadaud P, Horst O, Otto F, Eggeler G, George EP. Temperature dependencies of the elastic moduli and thermal expansion coefficient of an equiatomic, single-phase CoCrFeMnNi high-entropy alloy. J Alloys Compd 2015;623:348–53.

[8] Glienke M, Vaidya M, Gururaj K, Daum L, Tas B, Rogal L, et al. Grain boundary diffusion in CoCrFeMnNi high entropy alloy: kinetic hints towards a phase decomposition. Acta Mater 2020;195:304–16.

[9] Vaidya M, Pradeep KG, Murty BS, Wilde G, Divinski SV. Radioactive isotopes reveal a non sluggish kinetics of grain boundary diffusion in high entropy alloys. Sci Rep 2017;7(1):12293.

[10] Varvenne C, Luque A, Curtin WA. Theory of strengthening in fcc high entropy alloys. Acta Mater 2016;118:164–76.

[11] Coury FG, Wilson P, Clarke KD, Kaufman MJ, Clarke AJ. High-throughput solid solution strengthening characterization in high entropy alloys. Acta Mater 2019;167:1–11.

[12] Coury FG, Clarke KD, Kiminami CS, Kaufman MJ, Clarke AJ. High throughput discovery and design of strong multicomponent metallic solid solutions. Sci Rep 2018;8(1):8600.

[13] Laplanche G, Bonneville J, Varvenne C, Curtin WA, George EP. Thermal activation parameters of plastic flow reveal deformation mechanisms in the CrMnFeCoNi high-entropy alloy. Acta Mater 2018;143:257–64.

[14] Toda-Caraballo I. A general formulation for solid solution hardening effect in multicomponent alloys. Scripta Mater 2017;127:113–7.

[15] Xiao L, Huang P, Wang F. Inverse grain-size-dependent strain rate sensitivity of face-centered cubic high-entropy alloy. J Mater Sci Technol 2021;86:251–9.

[16] Maier-Kiener V, Schuh B, George EP, Clemens H, Hohenwarter A. Insights into the deformation behavior of the CrMnFeCoNi high-entropy alloy revealed by elevated temperature nanoindentation. J Mater Res 2017;32(14):2658–67.

[17] Lee D-H, Choi I-C, Yang G, Lu Z, Kawasaki M, Ramamurty U, et al. Activation energy for plastic flow in nanocrystalline CoCrFeMnNi high-entropy alloy: a high temperature nanoindentation study. Scripta Mater 2018;156:129–33.

[18] Leyson GPM, Hector LG, Curtin WA. Solute strengthening from first principles and application to aluminum alloys. Acta Mater 2012;60(9):3873–84.

[19] Otto F, Dlouhý A, Somsen C, Bei H, Eggeler G, George EP. The influences of temperature and microstructure on the tensile properties of a CoCrFeMnNi high-entropy alloy. Acta Mater 2013;61(15):5743–55.

[20] Sun SJ, Tian YZ, Lin HR, Dong XG, Wang YH, Wang ZJ, et al. Temperature dependence of the Hall–Petch relationship in CoCrFeMnNi high-entropy alloy. J Alloys Compd 2019;806:992–8.

[21] Schuh B, Mendez-Martin F, Völker B, George EP, Clemens H, Pippan R, et al. Mechanical properties, microstructure and thermal stability of a nanocrystalline CoCrFeMnNi high-entropy alloy after severe plastic deformation. Acta Mater 2015;96:258—68.

[22] Shahmir H, He J, Lu Z, Kawasaki M, Langdon TG. Evidence for superplasticity in a CoCrFeNiMn high-entropy alloy processed by high-pressure torsion. Mater Sci Eng, A 2017;685:342—8.

[23] Reddy SR, Bapari S, Bhattacharjee PP, Chokshi AH. Superplastic-like flow in a fine-grained equiatomic CoCrFeMnNi high-entropy alloy. Mater Res Lett 2017;5(6):408—14.

[24] Kilmametov A, Kulagin R, Mazilkin A, Seils S, Boll T, Heilmaier M, et al. High-pressure torsion driven mechanical alloying of CoCrFeMnNi high entropy alloy. Scripta Mater 2019;158:29—33.

[25] Zherebtsov S, Stepanov N, Ivanisenko Y, Shaysultanov D, Yurchenko N, Klimova M, et al. Evolution of microstructure and mechanical properties of a CoCrFeMnNi high-entropy alloy during high-pressure torsion at room and cryogenic temperatures. Metals 2018;8(2):123.

[26] Sun SJ, Tian YZ, Lin HR, Dong XG, Wang YH, Zhang ZJ, et al. Enhanced strength and ductility of bulk CoCrFeMnNi high entropy alloy having fully recrystallized ultrafine-grained structure. Mater Des 2017;133:122—7.

[27] Gludovatz B, Hohenwarter A, Catoor D, Chang EH, George EP, Ritchie RO. A fracture-resistant high-entropy alloy for cryogenic applications. Science 2014;345(6201):1153.

[28] Sun SJ, Tian YZ, Lin HR, Yang HJ, Dong XG, Wang YH, et al. Achieving high ductility in the 1.7 GPa grade CoCrFeMnNi high-entropy alloy at 77 K. Mater Sci Eng, A 2019;740—741:336—41.

[29] Soares GC, Patnamsetty M, Peura P, Hokka M. Effects of adiabatic heating and strain rate on the dynamic response of a CoCrFeMnNi high-entropy alloy. J Dyn Behav Mater 2019;5(3):320—30.

[30] Shabani M, Indeck J, Hazeli K, Jablonski PD, Pataky GJ. Effect of strain rate on the tensile behavior of CoCrFeNi and CoCrFeMnNi high-entropy alloys. J Mater Eng Perform 2019;28(7):4348—56.

[31] Liu G, Lu DH, Liu XW, Liu FC, Yang Q, Du H, et al. Solute segregation effect on grain boundary migration and Hall—Petch relationship in CrMnFeCoNi high-entropy alloy. Mater Sci Technol 2019;35(4):500—8.

[32] Han Z, Ren W, Yang J, Du Y, Wei R, Zhang C, et al. The deformation behavior and strain rate sensitivity of ultra-fine grained CoNiFeCrMn high-entropy alloys at temperatures ranging from 77 K to 573 K. J Alloys Compd 2019;791:962—70.

[33] Gali A, George EP. Tensile properties of high- and medium-entropy alloys. Intermetallics 2013;39:74—8.

[34] Moon J, Hong SI, Bae JW, Jang MJ, Yim D, Kim HS. On the strain rate-dependent deformation mechanism of CoCrFeMnNi high-entropy alloy at liquid nitrogen temperature. Mater Res Lett 2017;5(7):472—7.

[35] Thompson AW. Calculation of true volume grain diameter. Metallography 1972;5(4):366—9.

[36] Wei Q. Strain rate effects in the ultrafine grain and nanocrystalline regimes—influence on some constitutive responses. J Mater Sci 2007;42(5):1709—27.

[37] Wu Z, Gao Y, Bei H. Thermal activation mechanisms and Labusch-type strengthening analysis for a family of high-entropy and equiatomic solid-solution alloys. Acta Mater 2016;120:108—19.

[38] Langdon TG. Seventy-five years of superplasticity: historic developments and new opportunities. J Mater Sci 2009;44(22):5998.